U. Walzer and R. Hendel. Tectonic episodicity and convective feed-back mechanisms. Phys. Earth Planet. Int., 100:167-188, 1997b.

ELSEVIER

Physics of the Earth and Planetary Interiors 100 (1997) 167–188

PHYSICS OF THE EARTH AND PLANETARY INTERIORS

Tectonic episodicity and convective feedback mechanisms

Uwe Walzer *, Roland Hendel

Institut für Geowissenschaften, Friedrich-Schiller-Universität, Burgweg 11, 07749 Jena, Germany

Received 1 September 1995; accepted 12 March 1996

Abstract

The evolution of the Earth is characterized by irreversible processes: radioactive decay of the major heat-producing elements, thermal convection and chemical segregation. The prevailing heating from within and the temperature dependence of the viscosity are essential for thermal convection. In the present paper, the chemical and thermal evolution of the mantle and the generation of the continent material are represented by a two-dimensional and finite-difference Boussinesq convection model. We have incorporated the above-mentioned principal features in this model, a geochemical paper by Hofmann (1988, *Earth Planet. Sci. Lett.*, 90: 297–314) constituting our starting point for the distribution of the radionuclides. The concentration of the radionuclides and the viscosity are functions of the location and time developing according to our system of differential equations. Although the real Earth is a much more complex system, we have dared to make a comparison with observed geophysical and geological data; we obtain a depleted upper mantle and acceptable values for the heat flow on the surface of the Earth as well as for the distribution of temperature, viscosity and of the velocity of creep in the mantle. The ups and downs of the convective vigour of the model roughly resemble the supercontinental cycles, the world-wide distribution of mineral dates in time, the sea-level variations and the variations of a number of geochemical parameters. © 1997 Elsevier Science B.V.

1. Introduction

The igneous and metamorphic mineral date abundances do not show, in terms of space or time, a uniform distribution over the continents. If all of these data are plotted for all continents jointly versus time, that is, if one plots, for example, on the ordinate, the number of all mineral date localities which occur in a 10^7 year interval, pronounced maxima and minima are obtained (Gastil, 1960). There are periods in which large areas of continental crust are formed, interrupted by more quiescent periods. Very similar curve behaviours have been obtained by modern workers, e.g. Condie (1989). It is fair to assume that there must be a link between the chemical segregation leading to the formation of continental crust material, the recycling (anatexis) of granitic and granodioritic material and thermal mantle convection. In looking for such a link, we proceed from the assumption that the endothermic spinel–perovskite phase change at 670 km depth is promoting a two-layer convection state in the mantle. This means that we want to show with our model calculations that these episodes of enhanced magmatism and orogeny may be explained even if convective mantle avalanches (Machetel and Weber, 1991; Tackley et

* Corresponding author.

PII S0031-9201(96)03238-4

al., 1993) are not taken into consideration, and that a correct distribution in time of the maxima follows from our computed models. The purpose of this approach is not to deny the existence of the avalanches or their counterpart, the plumes penetrating the 670 km discontinuity, but to show that their significance for the continental evolution is possibly being overestimated. Thus, it is our view that the periods characterized by a considerable growth in the continental volume are closely related with the Wilsonian cycle and that the latter follows from the thermal evolution of the Earth, which is dominated by layered convection. In this connection, it has to be pointed out, too, that the majority of numerical studies of flushing events have been conducted for a constant or, at best, depth-dependent shear viscosity.

A link between mantle convection and mantle differentiation through the production of continental crustal rock has already been suggested by Spohn and Breuer (1993). The convection was calculated in this case in its parameterized form, whereby, in our view, certain feedback effects were excluded, which occur in our fully dynamic system and which are exactly the factors responsible for the generation of the maxima and minima of continental growth. Spohn and Breuer's result is nevertheless of great value, as it reflects evolution so to speak in a smoothed form.

The time-dependent convection model calculations show a strong dependence on the rheology (Christensen, 1984; Christensen and Yuen, 1989), the oscillations with a nonlinear rheology having a much greater magnitude. Meanwhile, the temperature- and pressure-dependent rheology of olivine has been introduced for the upper mantle (Schmeling and Marquart, 1993; Schmeling and Bussod, 1996), resulting in pronounced convective peaks associated with rising plumes or sinking blobs. Not only the Rayleigh number, but also the aspect ratio and the initial conditions have a considerable influence on the time behaviour of the convective flows in a two-dimensional model (Hansen and Ebel, 1988). It is for these and other reasons that the modelling of the time dependence of mantle convection poses such difficulties and may be solved only in principle, but not with respect to each and every detail.

The basic idea of the present paper is distantly akin to the work of Ogawa (1988, 1993, 1994). In his model, the mantle convection is represented by a two-component Newtonian fluid flow with fractionation of heat-producing elements into magma. The two components of Ogawa's fluid constitute a eutectic system. The mantle magmatism is modelled by the fractionation of the eutectic mixture. The mantle convection is the cause of pressure-release melting. The latter provokes the magmatism, which generates density differences dependent on the chemical composition.

In our view, the connection of the numerical results of convection computations with observed data for the real Earth constitutes an essential problem. Whereas Ritzert and Jacoby (1992) have established a link between the geoid and two-dimensional convection computations, we are attempting here to compare the evolution in time of convection models involving chemical segregation in a simplified form with the observed magmatic and orogenetic evolution of the Earth. We demand that, as far as they are known, the stream function, temperature, heat flux on the surface of the Earth, and the viscosity as a function of depth are also correctly approximated by the model.

2. Problem formulation

The mantle model used in this paper is an incompressible medium with internal heating. We use the Oberbeck–Boussinesq equations for infinite Prandtl number convection. The velocity v_k and the temperature T are functions of the location vector x_i and time t. They are calculated from the conservation of momentum

$$\rho\frac{\mathrm{d}v_k}{\mathrm{d}t} = \rho b_k + \frac{\partial\sigma_{ik}}{\partial x_i} \tag{1}$$

and conservation of energy

$$\rho\frac{\mathrm{d}u^*}{\mathrm{d}t} + \frac{\partial q_i}{\partial x_i} = Q + \sigma_{ik}\dot{\epsilon}_{ik} \tag{2}$$

Owing to the incompressibility, the horizontal component u and vertical component w of the velocity v_k can be represented by the scalar stream function ψ:

$$u = \frac{\partial\psi}{\partial z} \text{ and } w = -\frac{\partial\psi}{\partial x} \tag{3}$$

Table 1
Data on major heat-producing isotopes

Isotope	^{40}K	^{232}Th	^{235}U	^{238}U
ν	1	2	3	4
τ_ν (Ma)	2015.3	20212.2	1015.4	6446.2
$H_{o\nu}$ (W kg^{-1})	0.272×10^{-3}	0.0330×10^{-3}	47.89×10^{-3}	0.1905×10^{-3}
$a_{if\nu}$	0.000119	1	0.0071	0.9928

$\dot{\epsilon}_{ik}$ denotes the strain-rate tensor

$$\dot{\epsilon}_{ik} = \frac{1}{2}\left(\frac{\partial v_i}{\partial x_k} + \frac{\partial v_k}{\partial x_i}\right) \quad (4)$$

and σ_{ik} the stress tensor

$$\sigma_{ik} = -p\delta_{ik} + \lambda\dot{\epsilon}_{jj}\delta_{ik} + 2\eta\dot{\epsilon}_{ik} \quad (5)$$

As abbreviation, the substantial differentiation with respect to time $(\mathrm{d}\cdots)/(\mathrm{d}t) = (\partial\cdots)/(\partial t) + \boldsymbol{v}\cdot\nabla\cdots$ and the heat flux vector $q_k = -k(\partial T)/(\partial x_k)$ have been used, where ρ is the density, b_k the acceleration, p the dynamic pressure, α the coefficient of thermal expansion, and λ the volume viscosity.We let

$$\rho = \rho_o[1 - \alpha(T - T_o)] \quad (6)$$

be our kinetic equation of state. Via the dependence on the temperature T, the shear viscosity is a function of the location vector x_i and time t:

$$\eta = k_1 \cdot \exp(k_2 T_m/T) \quad (7)$$

the melting temperature T_m being composed by us after Ranalli (1991) from the dry solidus of peridotite for the upper mantle after Ito and Takahashi (1987), the melting curve of perovskite after Heinz and Jeanloz (1987) for the lower mantle up to a depth of 1500 km, and the melting curve of perovskite after Knittle and Jeanloz (1989) for the lower mantle below a depth of 1500 km. After the introduction of dimensionless variables (see Appendix A),

$$4\frac{\partial^2}{\partial x \partial z}\left(\eta\frac{\partial^2\psi}{\partial x \partial z}\right) + \left(\frac{\partial^2}{\partial z^2} - \frac{\partial^2}{\partial x^2}\right)\left[\eta\left(\frac{\partial^2\psi}{\partial z^2} - \frac{\partial^2\psi}{\partial x^2}\right)\right] = \mathrm{Ra}\frac{\partial T}{\partial x} \quad (8)$$

follows from the conservation of momentum, the conventional Rayleigh number

$$\mathrm{Ra} = \frac{\rho_o \cdot \alpha \cdot g \cdot \Delta T_o \cdot h^3}{\eta_o \cdot \kappa}$$

solely serving as a scaling variable. From the conservation of energy, the following equation is derived:

$$\frac{\partial T}{\partial t} + \frac{\partial\psi}{\partial z}\cdot\frac{\partial T}{\partial x} - \frac{\partial\psi}{\partial x}\cdot\frac{\partial T}{\partial z} = \frac{\partial^2 T}{\partial x^2} + \frac{\partial^2 T}{\partial z^2} + H(x,z,t) \quad (9)$$

the non-dimensional specific heat production H being calculated from

$$H = \sum_{\nu=1}^{4} a_{\mu\nu}\cdot a_{if\nu}\cdot H_{o\nu}\cdot\exp(-t/\tau_\nu) \quad (10)$$

The subscript ν denotes the radionuclides heating up the Earth (a value of one stands for the isotope ^{40}K, two for ^{232}Th, three for ^{235}U, and four for ^{238}U). $a_{\mu\nu} = a_{\mu\nu}(x,z,t)$ denotes the abundance of the element. We assume that the elements show a homogeneous distribution in the upper mantle and lower mantle at the beginning of the evolution of the Earth. Through chemical segregation and convective flow, however, the distribution of the heating sources is continually changing; the same is true for the distribution of shear viscosity. As the latter is variable by a few orders of magnitude dependent on the temperature field, we consider constant-viscosity models not to be particularly well suited for describing the thermal and chemical evolution of the mantle. $a_{if\nu}$ denotes the isotopic abundance factor, which is non-dimensional anyway. τ_ν is the period of time after which $1/e$ of the original mass of the isotope is still left. $H_{o\nu}$ is the specific isotopic heat production 4.55×10^9 years ago. $H_{o\nu}$ must be made dimensionless. The above-mentioned material constants are given in Tables 1 and 2. The values shown in the first table have been calculated by us from data taken from Van Schmus (1989), and those given in the second one follow from the geochemical two-stage model of Hofmann (1988), which has been slightly modified by us. If the normalized concentration is plotted versus the compatibility of the elements, a

Table 2
The abundances $a_{\mu\nu}$ of the major heat-producing elements according to Hofmann (1988)

Marker index	(1)	(2)	(3)	(4)	(5)
Reservoir	Primordial mantle (ppm)	Oceanic crust (ppm)	Continental crust (ppm)	Res 1 (ppm)	Res 2 (ppm)
K	258.2	883.7	9100	201.48	161.98
U	0.0203	0.0711	0.91	0.0146	0.0112
Th	0.0813	0.1871	3.5	0.0594	0.0529

precisely reversed trend is obtained with respect to the continental crust, on the one hand, and mid-ocean ridge basalt (MORB), on the other hand, for the abscissa sections characterized by highly incompatible elements (Rb, U, Th, Ba, Cs, etc.) and moderately incompatible elements up to the rare-earth elements. Hofmann—and other workers—concluded from this that the continental crust and a depleted part of the mantle complement each other geochemically. The primordial primitive mantle would first differentiate at an early stage of the Earth's evolution into the continental crust and a first depleted residue (res 1). The rest of the primordial mantle would be left under the latter. From the first residue, the oceanic crust would then be formed, and a second residue, which is also depleted in incompatible elements, and a residual amount of the first residue. The numerical values given in Table 2 will now be used in our dynamic model. The major heat-producing isotopes are represented by tracers entrained in the stream. A certain number of runs performed by us are based on Type 1 markers, which initially were uniformly distributed over the whole mantle. In other runs, we assumed that, for depths smaller than 670 km, the $a_{\mu\nu}$ of all four radionuclides are increased by the intensification factor k_8. Although this yields thermally acceptable values, it still leads to a depleted upper mantle for the geological present. The number $z_{\mu\nu}$ of Type 1 tracers required for the creation of a Type 3 tracer are calculated for the model K149 and the upper mantle from

$$k_8 \cdot a_{\mu\nu}^{(1)} + z_{\mu\nu}^{*}\left[k_8 \cdot a_{\mu\nu}^{(1)} - a_{\mu\nu}^{(4)}\right] = a_{\mu\nu}^{(3)} \qquad (11)$$

and

$$z_{\mu\nu} = \mathrm{round}\left(z_{\mu\nu}^{*}\right) \qquad (12)$$

For the lower mantle, $k_8 = 1$ will have to apply. If the viscosity drops below a critical value f_6 in a sufficiently large area, we assume that the continental Type 3 tracers are carried upwards by volcanism. There, a Type 1 tracer is transformed in a strip of D_c width into a Type 3 tracer. The D_c strip represents the future lithosphere. The clusters of Type 3 tracers present on the surface represent the continents formed through chemical segregation. Eq. (11) ensures the conservation of the number of individual radioactive parent nuclei and radiogenic daughter nuclei. Compared with the slow currents of the solid-state creep of the solid matrix of the mantle, the melt is practically rising instantly. The motivation of the simplified segregation mechanism and the detailed procedure are given in Appendix A and Appendix B.

Free-slip boundaries and an isothermal 300 K upper surface are assumed for all model computations of this paper. The other boundaries have a zero heat flux, i.e. the temperature may develop there freely in conformity with the laws of the model system. As is well known, there is a sharp cutoff in seismicity in the Earth's mantle at a depth of 670 km (Billington, 1978), a seismic velocity increase by about 6% and a negative Clapeyron slope of possibly $(-3.0 \pm 1.0)\,\mathrm{MPa\,K^{-1}}$ (Akaogi and Ito, 1993).

Across the endothermic phase transition, a considerable change in the viscosity has to be expected, too. Therefore, we heuristically introduce $w = 0$ for a depth of 670 km; the reasons for this will be explained in greater detail in another paper. In accordance with common practice in numerical mantle convection computations, a small disturbance $T_s(x,z)$ is superimposed on the initial temperature $T_o(x,z)$ to set the flow in motion.

$$T_s(x,z) = A_s \cdot \sin\left(\frac{\pi \cdot x}{x_{max}}\right) \cdot \cos\left(\frac{\pi \cdot z}{2 \cdot z_{max}}\right) \cdot T_m(z) \qquad (13)$$

has been used, with $A_s = 0.01$. We have assumed that the starting temperature $T_o(x,z)$ of the mantle

was 70% of the melting temperature $T_m(z)$. The reason behind this choice was the desire to let the evolution of the mantle begin with a moderate, constant viscosity throughout the model.

3. Results

3.1. Results and comparison with geophysical data

The equations given above are solved using a finite difference scheme. The results shown are stable within a certain k_8 range. Figs. 1–5(c) apply to $k_8 = 5.551$. In Fig. 1, the evolution of important mean values is summarized. From the top downwards, the heat flux calculated at the surface, the kinetic energy of the convective flows of the whole mantle, the amount of transformed continent tracers per unit time (25 Ma), and the averaged mantle temperature are shown as a function of time. Pollack et al. (1993) averaged 24 774 observations from heat flow measurements at 20 201 sites. The observations cover 62% of the Earth's surface, if a $5° \times 5°$ grid is used in the computation. The global mean today is $87\,\mathrm{mW\,m^{-2}}$, the mean heat flux of the oceans $101\,\mathrm{mW\,m^{-2}}$. These values are well approximated by the upper panel of Fig. 1. The kinetic energy is intended to serve only as a measure for the convective vigour, its fluctuations being an inherent feature of the model caused by feedback mechanisms. The early Archaean more than 3400 Ma ago only shows upper-mantle convection. During the Proterozoic and Phanerozoic, however, there was thermal convection in both the upper and lower mantle. Only the deeper part of the lower mantle exhibits a very sluggish behaviour, because viscosity strongly increases with depth. In third panel of Fig. 1, attention must be paid to the fact that the whole primordial mantle is represented by 161×161 markers and that there is a linear relationship between the plotted number of markers per 25 Ma and the newly depleted mantle volume.

The early principal maximum of the third panel is in good agreement with Warren's thesis (Warren, 1989) that the main mass of the continental material has been formed by chemical segregation from the

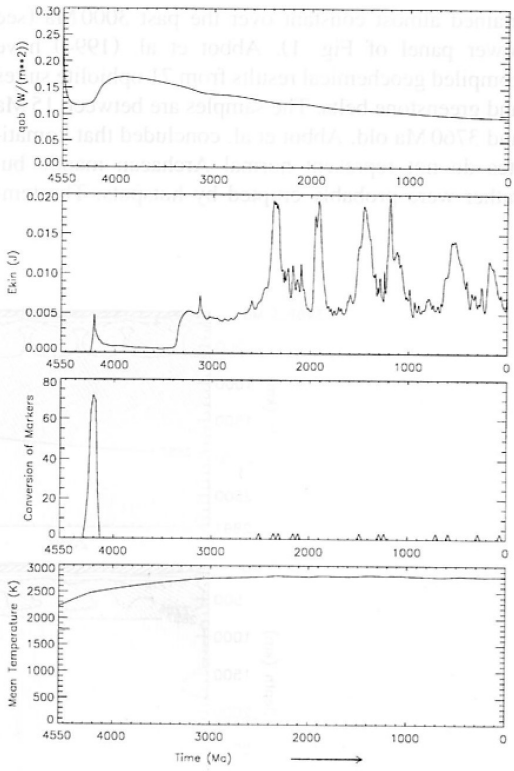

Fig. 1. The upper panel shows the evolution of the averaged heat flux on the surface of the model Earth. In the second panel, the ups and downs of the kinetic energy of mantle convection may be seen. The third panel shows that the original production of continent material took place for a large part during the early Archaean. The lower panel gives the temperature averaged over the whole mantle as a function of time. $k_8 = 5.551$.

mantle during the earliest Archaean and that an ever-increasing percentage of palingen material is contained in subsequent additions to the continents through the accretion of island arcs and terranes, through anatexis, etc. According to Dasch et al. (1988), the principal period of the lunar crustal genesis dates back 4500–4200 Ma, whereas our dynamic model of the Earth yields a principal period of continental crust formation dating back 4300–4100 Ma. Whereas the mean global heat flux on the Earth's surface monotonously decreased during the past 3900 Ma, the mean mantle temperature re-

mained almost constant over the past 3000 Ma (see lower panel of Fig. 1). Abbot et al. (1994) have compiled geochemical results from 71 ophiolite suites and greenstone belts. The samples are between 15 Ma and 3760 Ma old. Abbot et al. concluded that komatiites do not represent normal Archaean mantle but rather were probably erupted by hotspots. The temperature change would be less than previously thought. Those workers believe that the relative proportion of hotspot magmas has remained nearly constant over geologic time. These results are in good concordance with the temperature–time curve of the present model (Fig. 1, fourth panel).

The upper panel of Fig. 2 shows that the lower

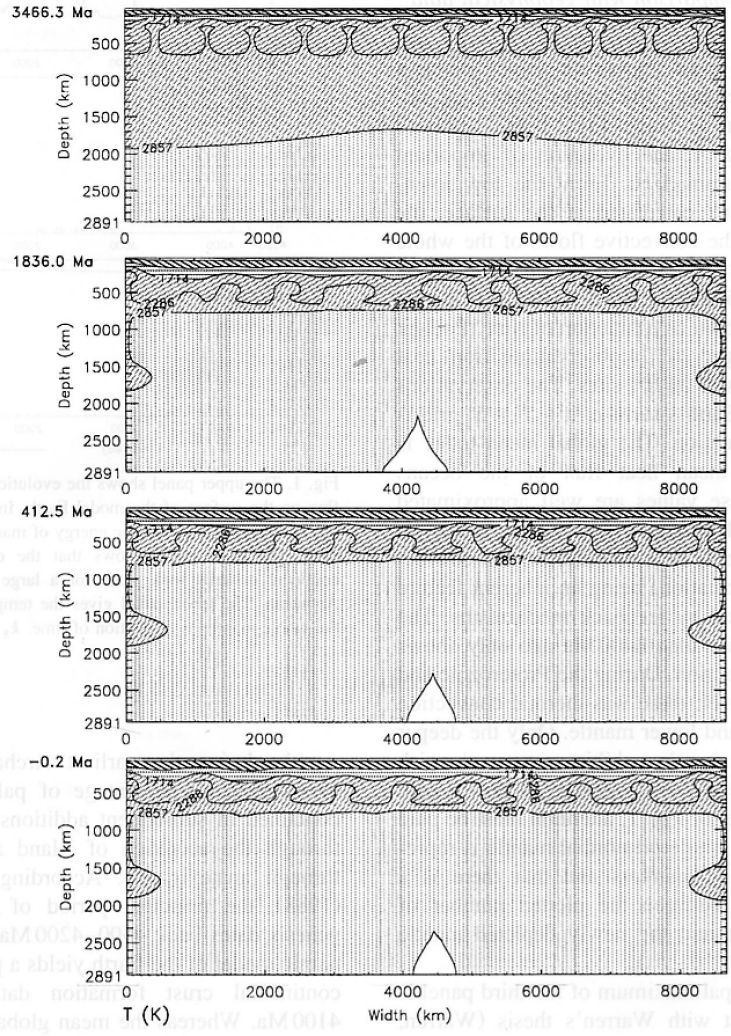

Fig. 2. A few snapshots of the evolution of temperature (in K). The age of temperature distribution is always given on the left of the ordinate.

mantle is at first gradually heating up, whereas a large number of convection cells already exist in the upper mantle. The following three panels point to cold downflows at the edge and a hot diapir in the middle. The spatial distribution is, of course, an artefact owing to the side walls of the model, which do not exist in reality. The shear viscosity is not considered to be constant with respect to space or time. The left four panels of Fig. 3 show the dynamic development of viscosity. This distribution has a great influence on the velocity distribution, whose development in time is represented in a few snapshots in Fig. 4 by the stream function ψ. Everywhere, we can see separate cycles in the upper and lower mantle, the lower mantle starting to flow only during the Archaean. The right four panels of Fig. 3 show the laterally averaged shear viscosity as a function of depth for a number of selected times. The depth of 670 km shows at any one time a relative maximum of the viscosity, constituting an obstacle for plumes with small diameters, which could come from below, or for subducting slabs, coming from above. Neither plumes of small diameter nor slabs in a narrower sense of the word have so far been incorporated in the model.

Fig. 5 shows the chemical composition with respect to the heat-producing radionuclides. The Type 1 markers (see Table 2) represent the primordial mantle, Type 3 markers represent the continental crust, and Type 4 markers the Residue 1, a form of

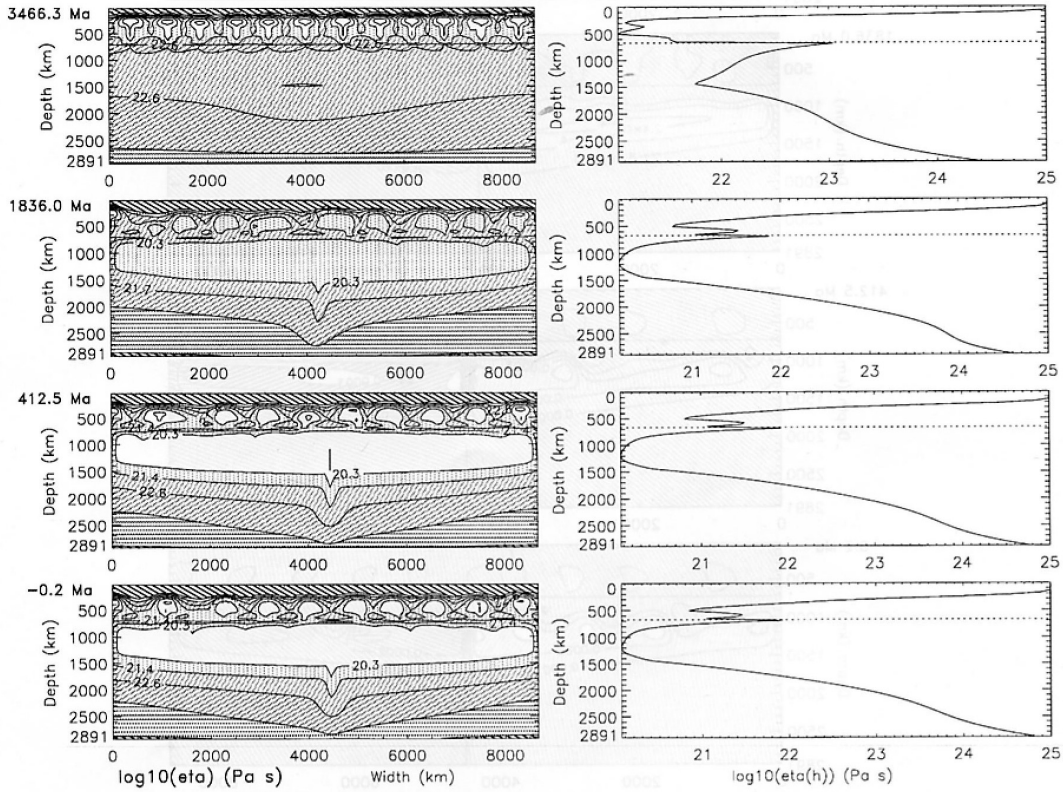

Fig. 3. A few snapshots of the development of viscosity (in Pa s) are given at the left. At the right, the viscosities averaged over the width as a function of depth are given for the same age values as for the snapshots at the left.

depleted mantle. Though much continental material has already been formed at an age of 3466.3 Ma (Fig. 5(a)), the lower mantle has not yet experienced convective movements; consequently, the Type 1 markers there are still in their initial position. The lower mantle is in motion, however, at 1836.0 Ma (Fig. 5(b)), only its lowermost part—apart from a plume—still being movable only to a relatively limited extent. The same picture is obtained in a similar form for an age of −0.2 Ma (Fig. 5(c)), that is to say, practically for the present. Only the layer in the lowermost mantle, which has moved relatively little, has become somewhat thinner.

We will describe in another paper the influence of the variation of the parameters on the evolution of the model, and we confine ourselves here, using Fig. 6(a), to showing only the influence of k_8 on the evolution of the kinetic energy of mantle convection.

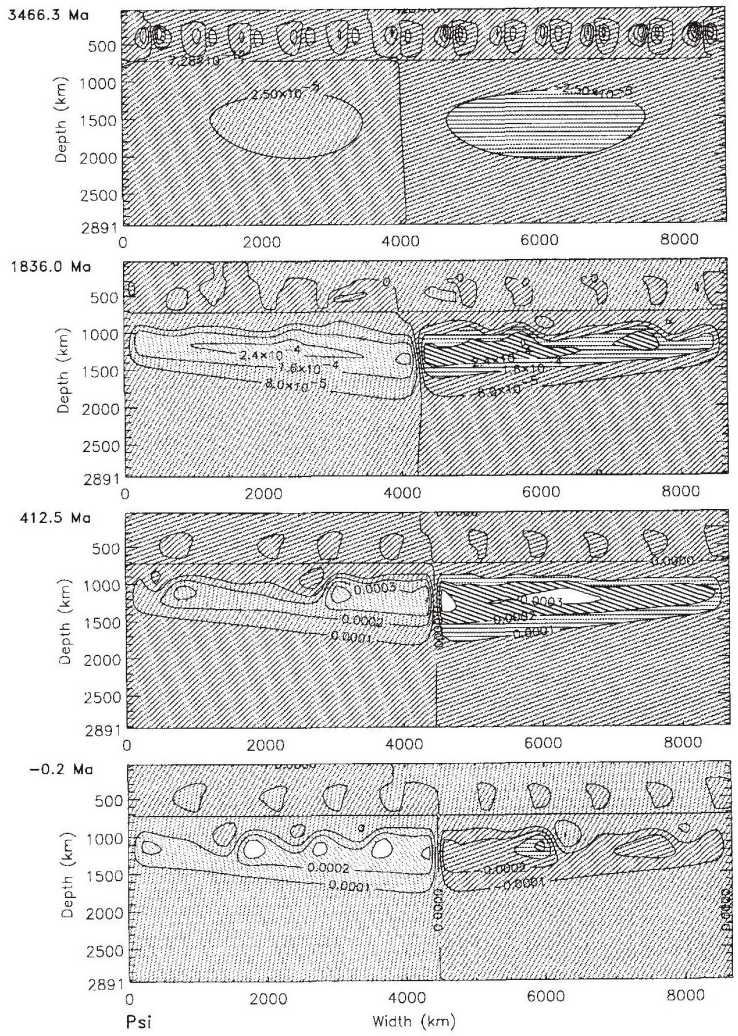

Fig. 4. A few snapshots of the evolution of the stream function for the same age values as in Fig. 2 and Fig. 3.

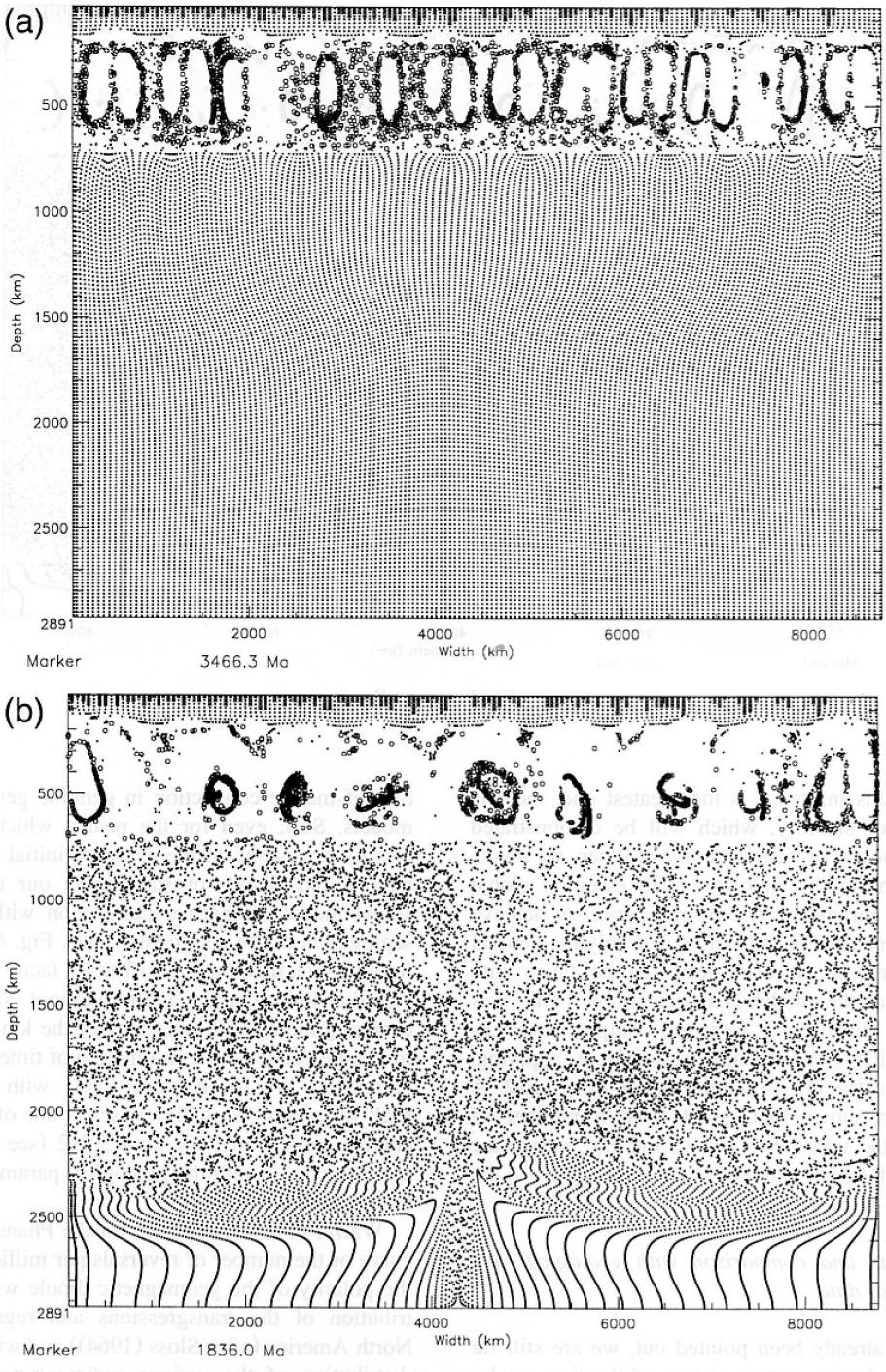

Fig. 5. The evolution of the chemical composition of the mantle. ●, Primordial mantle; ∗, continental crust; ○, depleted mantle (Res 1).

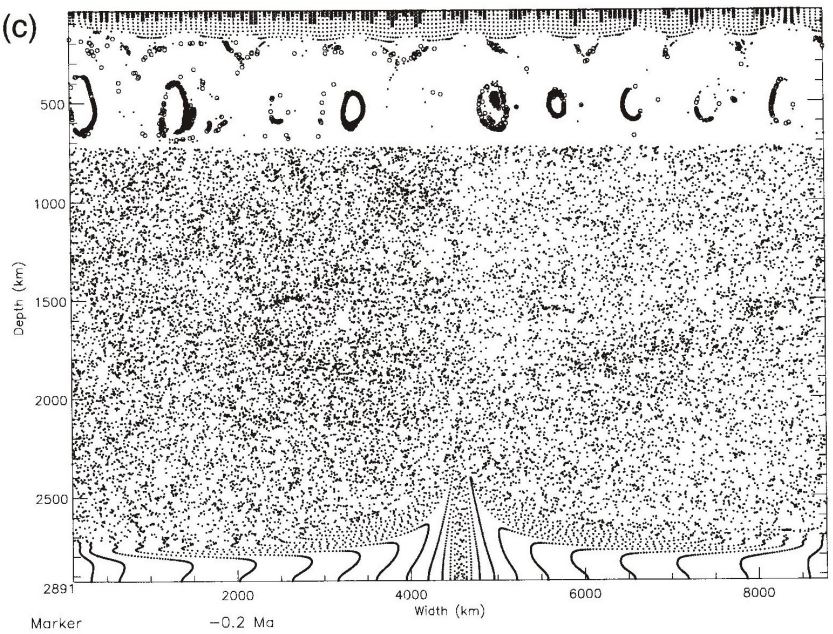

Fig. 5 (continued).

Although this influence is the greatest one, there is an island of stability, which will be demonstrated here by means of four examples. When we make comparisons in the following with essential global geological parameters, we do not expect to achieve precise agreement of the phases, but only the general curve behaviour. It also needs to be taken into account that the model is rather simple. This was necessary, however, to limit the computational expenditure. Fig. 6(b) is analogous to Fig. 1, applying, however, to the intensification factor $k_8 = 5.512$. A comparison shows that, apart from a number of details in the time behaviour of the E_{kin} curve, the variation of k_8 has caused only minor changes in the results.

3.2. Results and comparison with geological and geochemical data

As has already been pointed out, we are still far away from having a true picture of the time evolution of mantle convection in genuine geodynamical models. Still, even for the results which are most clearly dependent on the assumed initial values, we have found islands of stability in our two-dimensional model of thermal convection with chemical segregation of the continents. Thus, Fig. 6(a) shows, for example, that the intensification factor k_8 may be varied within certain limits without significantly changing the overall behaviour of the kinetic energy of mantle convection as a function of time. The other parameters are much more stable with respect to such variations. We will now select one of these E_{kin} curves, namely that for $k_8 = 5.512$ (see Fig. 6(b)), and compare it with the geological parameters given by other workers.

Walzer (1981) compared, for the Phanerozoic, the curve of the number of reversals per million years of the polarity of the geomagnetic dipole with the distribution of the transgressions and regressions in North America (after Sloss (1964)) and with the time distribution of the various sediment types on the

Eastern European platform after Ronov et al. (1969). It turned out that the three large-scale transgressions corresponded exactly to the episodes during which the geomagnetic dipole rarely reversed its polarity or did not reverse it at all. This showed, even in the absence of a more detailed theory, that there are processes involving the whole mantle (e.g. whole-mantle convection or layered mantle convection). These processes form the link between the hydromagnetic outer-core convection and the movements of the lithosphere mentioned above. When we repeat this comparison with more modern material, we arrive at the same conclusion: the mean reversal rate after Merrill and McFadden (1990) shows that no reversal in the polarity has taken place simultaneously with the large-scale transgression between 80 and 120 Ma. Marzocchi et al. (1992) concluded, in agreement with the above considerations, that there is a strongly negative correlation between geomagnetic reversals and long-term sea-level variations for the last 150 Ma.

The sea-level curves, which are fairly well known for the Phanerozoic (Vail and Todd, 1980; Hallam, 1984), have been schematized somewhat by Nance et

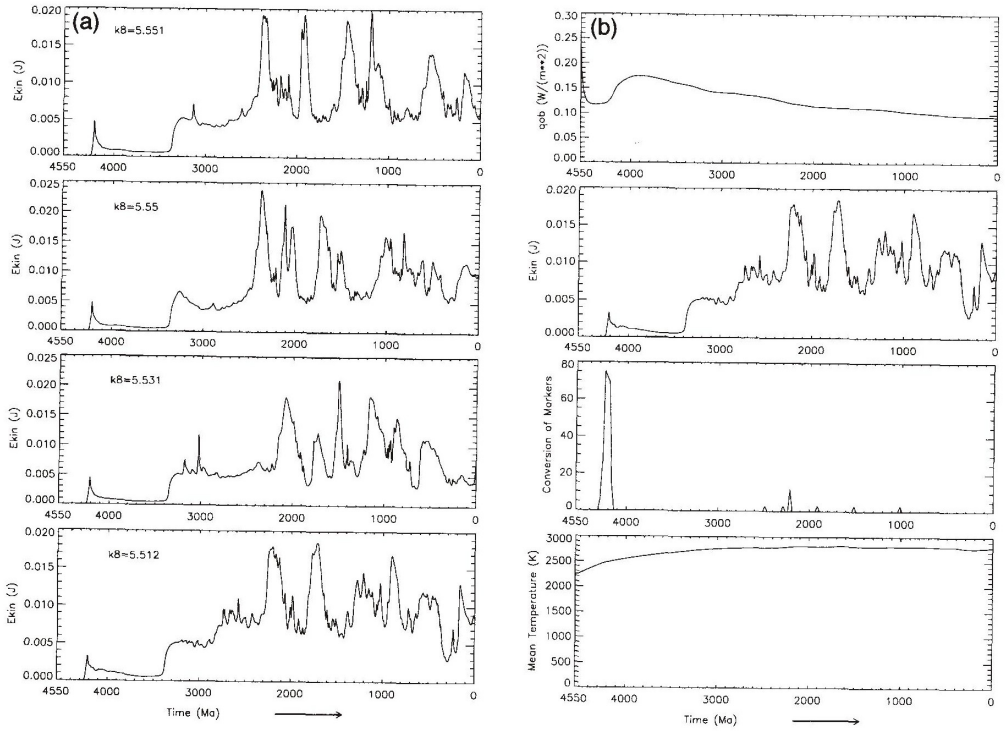

Fig. 6. (a) Diagrams showing the kinetic energy of mantle convection vs. geological age. The influence of the variation of the intensification factor k_8 becomes clear in a comparison of the curves. Its influence on other parameters such as the temperature and even viscosity is considerably lower. (b) Time series of our evolution model with an intensification factor $k_8 = 5.512$. The age is plotted towards the left on the abscissa. First panel: the heat flow q_{ob} averaged over the surface of the Earth. Second panel: the kinetic energy of convection averaged over the whole mantle. Third panel: conversion of markers or formation of continental crust from mantle material and, consequently, without rejuvenation. Fourth panel: temperature averaged over the whole mantle.

al. (1986), Nance et al. (1988) and correlated with the Wilson cycle. Their curve of the water depth at the shelf break after the fragmentation of the supercontinent (Pangaea) shows a strong rise by about 500 m. First, shallow marine clastics, and later marine chemical precipitates are deposited on the shelf and platform. Low pole-to-equator thermal gradients prevail in the climate. As the newly formed Atlantic-type oceans age and expand, this newly formed sea bottom will sink deeper. As a consequence, the sea-level will start to fall again during the late fragmentation phase. Collisions between the continents will then episodically produce a new supercontinent, which combines (almost) all the continental material. It produces large volumes of clastics. Orogenesis causes the formation of thicker continental packages, so that the surface of the continent will be higher. This elevation is enhanced even further by the heat accumulation under the supercontinent. Similarly to Africa at present, it is lifted by a few hundred metres. At the end of the Pangaea period, intercontinental rifts initiating a new fragmentation period are forming. There are obviously two types of orogeny. One type is the result of ocean crust subduction, e.g. at the Andes, and is rather uniformly distributed over the time axis. The other type is caused by continent-to-continent collision, e.g. in the Himalayas. It merges continents anew and is limited to certain periods characterized by subsequent regression. These regressions are caused by the isostatic uplift of the thickened continental crust and make themselves felt in the global sea-level curve. In Fig. 7 (lower part of upper panel), the evolution of the sea-level, as determined from geological observations, is plotted against the time axis after Worsley et al. (1986). Underneath, our curve of the evolution of the kinetic energy of mantle convection is shown. Although the lateral displaceability of the continents, which have been produced through segregation in the model, has not yet been fully implemented in our model, its thermal-convective mechanism and chemical differentiation mechanism create a curve with the same number of principal maxima. The position of the phases is only roughly in agreement, but the frequency content is very similar. In other models, we have also produced such curves solely through the lateral displaceability of the continents (retarding the heat removal). This comparison shows that not only the mechanism described by Worsley et al. (1986) with the help of words, that is to say, without making use of dynamic calculations, but also our convection–segregation mechanism may lead to this result. A combination of our convection–segregation mechanism and the continent-displaceability model appears to be promising to us, but will still have to be implemented in the form of a model (in the sense of theoretical physics and numerical mathematics) to substantiate this assumption.

Fig. 7 shows in its upper part a number of further correlations. On the left ordinate, the solar luminosity and the CO_2 content of the atmosphere are plotted with respect to the present level, which is designated by unity. The arrows represent biotic innovation episodes. The heights of the arrows indicate the ordinate values. The atmospheric oxygen level and the carbon-to-phosphorus burial ratio can be seen from the right-hand ordinate. The periods with supercontinents combining the entire continental material are defined by S1–S6 on the upper abscissa. The first known glaciation occurred at 2650 Ma (Harland, 1983), and further studies by Lovelock and Whitfield (1982) show that the temperature averaged over the Earth's surface has not exceeded approximately 25°C since then. This provides the justification for the assumption of such a constant temperature, in terms of time, on the surface of our computed model. F1–F6 define the beginning of the fragmentations, which must be viewed not only in terms of a mechanical and thermal repetition of the same process, but also in the sense of chemical and biotic innovations. This is to say that, similarly to with radioactive decay and the chemical segregation of the continents contained in our model, we have to do here with irreversible processes and, thus, a genuine evolution, onto which episodic processes, caused by feedbacks, are superimposed. The glacial interval at 2300 Ma coincides with the major abundance of banded iron-formation (James, 1983) in conjunction with an accelerated differentiation of large-ion lithophile elements into the continental crust. The fragmentation of the second supercontinent (F2) shows the earliest aulacogens. The areas which stabilized between 1900 Ma and 1700 Ma make up 74% of the pre-1600 Ma continental area (Patchett and Arndt, 1986); half of it, however, is recycled Archaean material. Condie (1989), too, confirmed

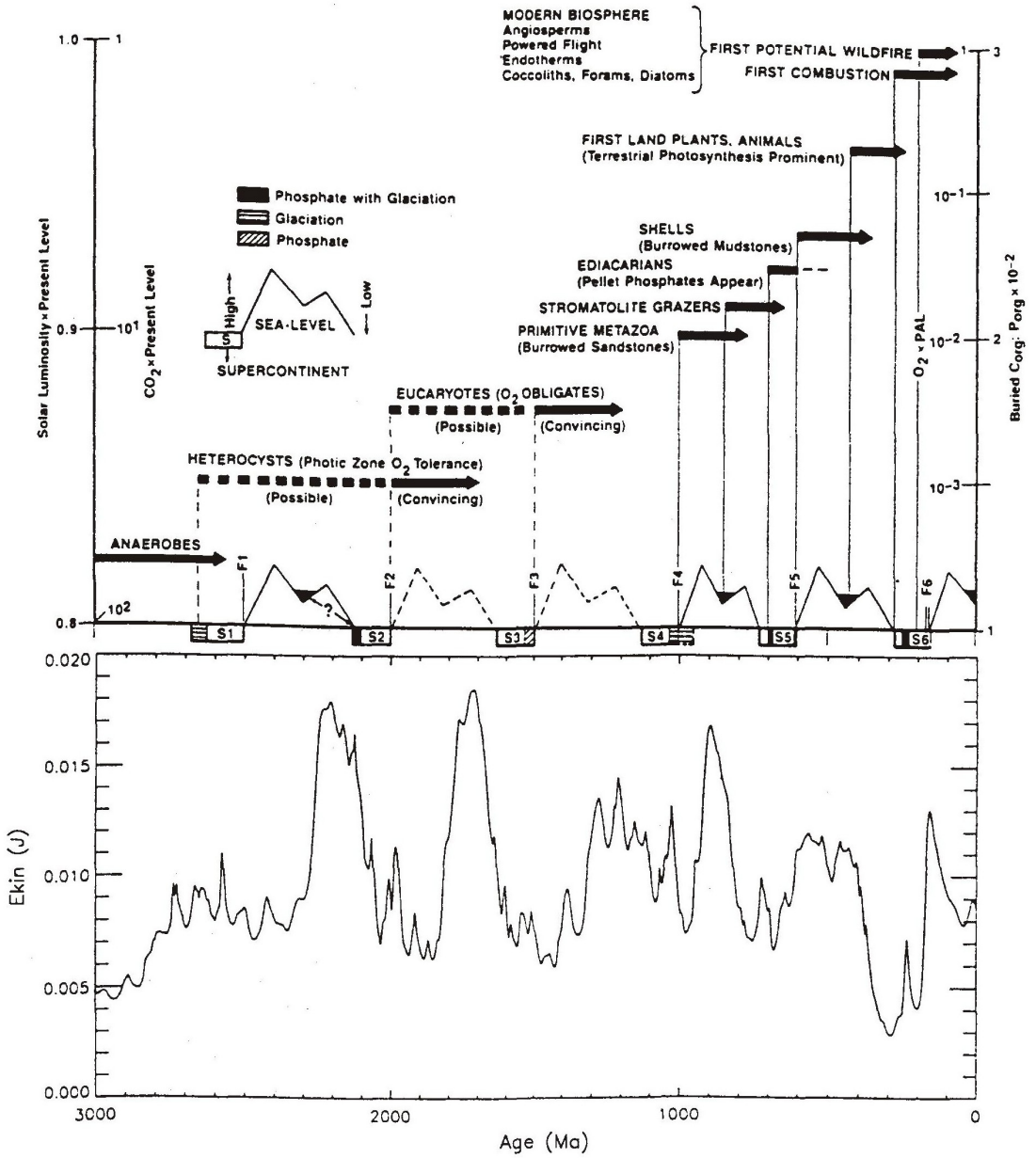

Fig. 7. Supercontinent cycles, biotic innovations, solar luminosity, CO_2 and O_2 levels of the Earth's atmosphere, C-to-P burial ratios after Worsley et al. (1986) at top are compared with the E_{kin} curve of our mantle convection–segregation model (this work, at bottom).

that we have to do here, as in the case of the 2600-Ma-old cycle, with world-wide periods of orogeny and crustal formation. These first two cycles correspond to the first two large maxima of our E_{kin} curve. The large maxima of the E_{kin} curve in general are generated by an intensification of the convective flows in the upper mantle and in the upper part of the lower mantle. The last one and a half Wilson cycles of the Phanerozoic are well known. The preceding supercontinent started to disintegrate 1000 Ma ago through rifting. Rogers et al. (1995) made an attempt to study in detail the correlation existing between the continental fragments of Rodinia.

Fig. 8(a) shows a comparison of our curve of time variations of the kinetic energy of mantle convection at the top and the igneous and metamorphic mineral dates against age after Gastil (1960) at the bottom. The time is subdivided into intervals of 10 my. The given ordinate is defined by the number of mineral date localities occurring during that time span. Naturally, in the case of younger ages, the main mass of the material has been produced through rejuvenation from older continental crust. This is also reflected in our model in the curve of the conversion of markers (see Fig. 6(b), third panel). Though an agreement of the phases of maxima cannot be observed everywhere, there is conformity in the frequency content and overall behaviour of the curve, so that it is still our hope that our model is appropriately covering essential features of mantle convection, the chemical differentiation of the continents and generation of the depleted mantle reservoir. A similar distribution of the world-wide mineral date abundances has been reported by Sutton (1967) and Condie (1989) for North America and the Baltic Shield (see Condie's Fig. 10.22, at bottom). Condie's list of North American orogenies (Condie, 1989) closely resembles the old Gastil curve. The initiations of the Shebandowan greenstone belt and of the Batchawana greenstone belt are both dated at 2730 Ma, the Grenville at 2280 Ma, Wopmay at 1900 Ma, Penokean at 1850 Ma and Green Mountain at 1750 Ma. The last three cluster in the first very high maximum of the Gastil curve. The Taconic dates at 450 Ma and Antler at 375 Ma. This corresponds to the last completed Wilson cycle and can also be clearly seen in the Gastil curve as a group of maxima. The Nevadan occurred at 160 Ma and the Laramide orogeny at 80 Ma. This corresponds to the last sharp maximum of the Gastil curve. Both groups can also be clearly identified in our E_{kin} curve.

Fig. 8(b) compares our time dependence of the kinetic energy of mantle convection (at the top) with the world-wide distribution of the mineral ages, which were determined with the help of U–Th–Pb methods after Gastil's compilation (Gastil, 1960). Here, too, a reasonable agreement of the frequency content and overall character of the curves can be noticed.

It may be worth noting at this point that the times of increased kinetic energy of mantle convection need not necessarily become apparent on all continents in the form of collisions and the associated orogenies (i.e. folding, regional metamorphism and granodioritic plutonism). Though collisions are more probable at times of increased flow velocities, such collisions may well not take place on some continents, depending on their initial positions. Even if, according to Condie (1989), a number of younger mineral date abundance periods cannot be observed world-wide simultaneously on all continents, it is still conceivable that increased velocities occurred in the mantle around the globe also at these times.

To avoid misunderstandings, it should also be pointed out that our episodes with an increased kinetic energy of the mantle flow, which become apparent in the form of episodically (and, thus, not strictly periodically) distributed Wilson cycles and of an increased magmatic and orogenetic activity in the continents, cover a considerable time span. They should by no means be mistaken for Stille's short-time rapid world-wide orogenic episodes (Stille, 1944). Whether these actually exist (Rampino and Caldeira, 1993), or whether the individual orogeny is a continuous process, and angular discordances are only mistaken at certain locations for episodes of deformation (Şengör, 1990) is of secondary importance and will not be discussed here.

The succession of the observed maxima of the sea-level curve (Fig. 7, centre), of the observed continental break-ups (Fig. 7) and of the observed high intensity of global magmatism (Fig. 8(a) and Fig. 8(b)) has no periodicity in a narrower sense, i.e. the distances of neighbouring major peaks are not equal. The same applies for the curve of the kinetic energy $E_{kin}(t)$ which has been computed by the

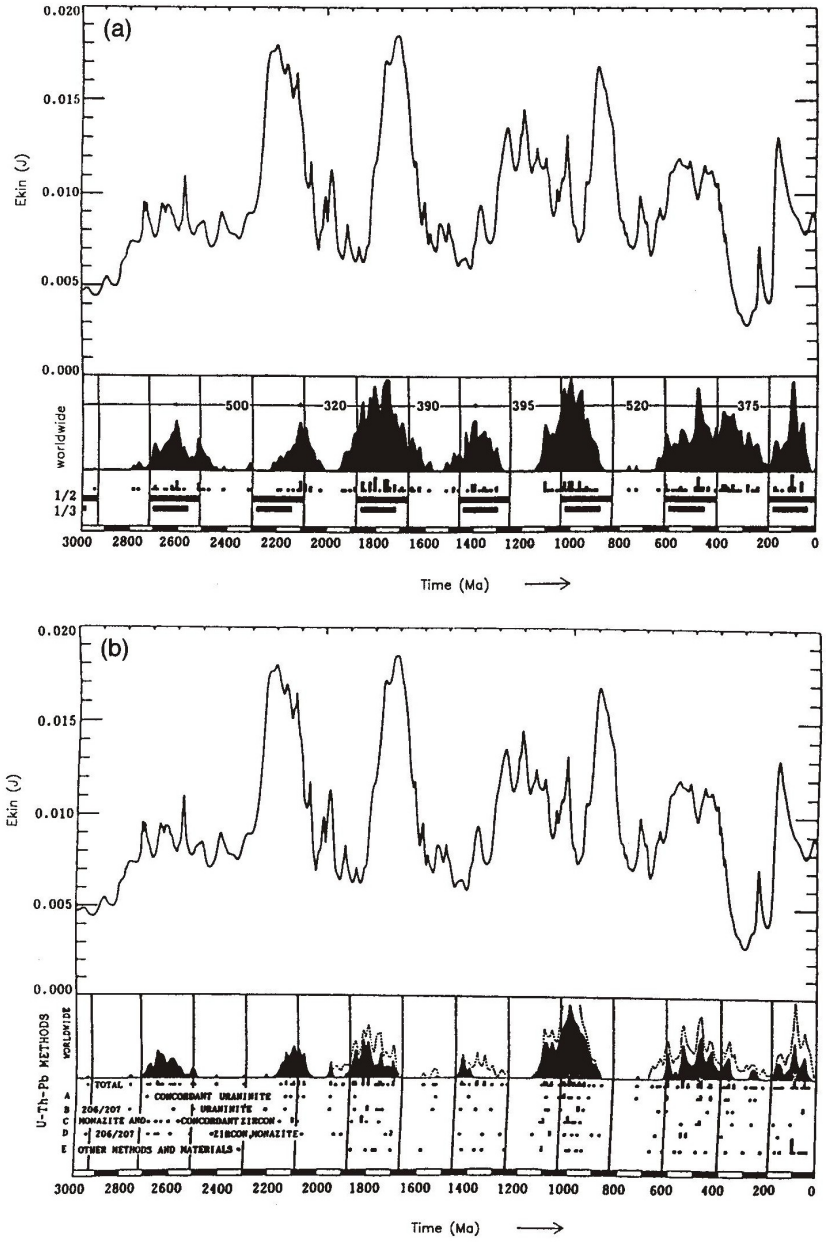

Fig. 8. (a) Comparison of the kinetic energy of our mantle model (at top) with the world-wide distribution of mineral dates in time after Gastil (1960), at bottom. (b) Comparison of the kinetic energy E_{kin} of our model (at top) with the mineral dates determined with the help of U–Th–Pb methods (at bottom).

model. The relationship of these observed and computed curves (number and position of main maxima, etc.) is by no means trivial but striking. Essential improvements can be expected if the possibility of lateral displacements of the continents (Gurnis, 1988) and the existence of subducting slabs (Zhong and Gurnis, 1994) are included in the model not only implicitly but in a more direct manner. The present paper shows that essential features of the Wilson cycle can be derived from the non-steady-state convection and from the fractionation of our model. It is not in the least surprising that at elevated sums of the velocity magnitudes of the convection, augmented magmatism occurs, because, at those periods, it is more probable to observe plate collisions, anatexis, regional metamorphosis, a regionally elevated heat flow, etc.

Titley (1993) has shown that stratabound Phanerozoic metal-sulfide ore deposits are closely linked with certain events of the Wilson cycle. He was able to demonstrate particularly well for volcanogenic massive sulphide (Cu, Pb, Zn) ores that their occurrence is tied to high sea-levels in the Wilson cycle. He mentioned an attempt to construct Proterozoic Wilson cycles on the basis of the descriptions by Windley (1984). In Fig. 9, this hypothetical sea-level curve (at the bottom) is compared with $E_{kin}(t)$ curves of our model (at the top). In the dotted rectangles underneath, the principal dike swarms are shown for the purpose of comparison. It can be clearly seen that the curve behaviours show some similarity.

Fig. 10 compares for the Phanerozoic the time sequence of our E_{kin} curve (at the top) with that of the mean sea-level. The lower continuous line shows the continental freeboard after Hallam (1984), and the dashed curve shows the same parameter after Vail et al. (1977). Hallam's curve has been derived from flooding–hypsometry data, whereas Vail's results have been obtained from seismic stratigraphy.

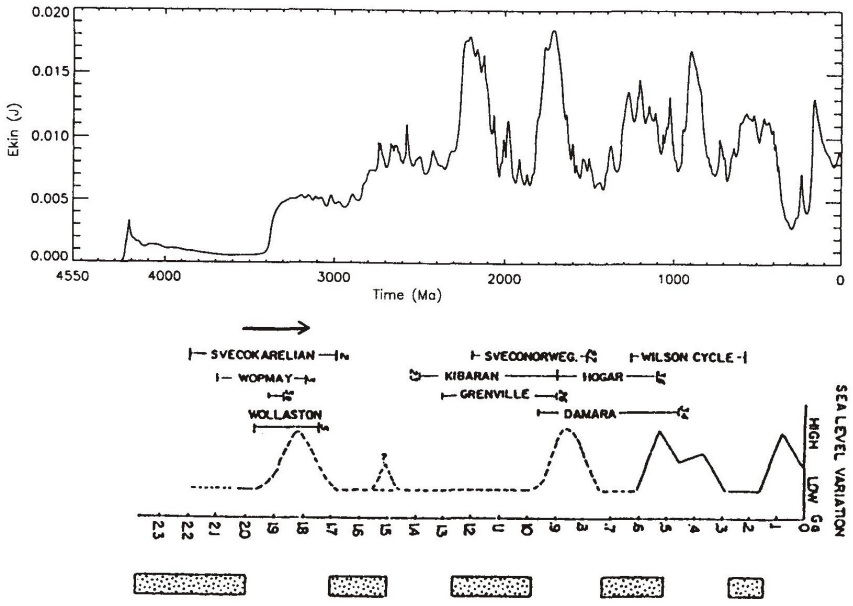

Fig. 9. Comparison of the sea-level variation after Titley (1993) (shown in the bottom part of the diagram) with the variation of the kinetic energy of mantle convection (this work, upper part of diagram).

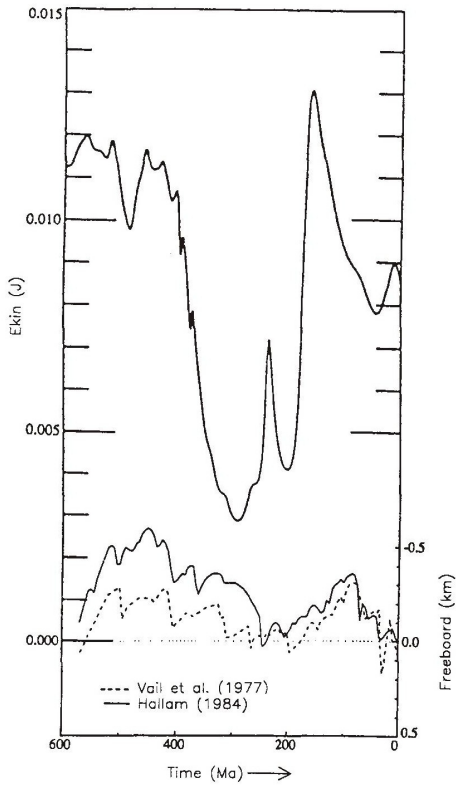

Fig. 10. Comparison of the E_{kin} curve of mantle convection (this work), at top, with Phanerozoic sea-level curves after Hallam (1984) and the dashed curve after Vail et al. (1977).

In addition to those workers, a number of other researchers see a connection between these large cycles of sea-level variations and continent collisions, the accretion of a supercontinent and the subsequent fragmentation of the supercontinent (Hoffman, 1990). Since it is our view that the supercontinent cycles are generated by mantle convection, the good correlation with the E_{kin} curve is worth noting only because of the simplicity of our convection model.

The lower part of Fig. 11 shows the stratabound ore distribution in time for the Phanerozoic after Titley (1993), the middle part the sea-level curve after Nance et al. (1986), and the upper part our time

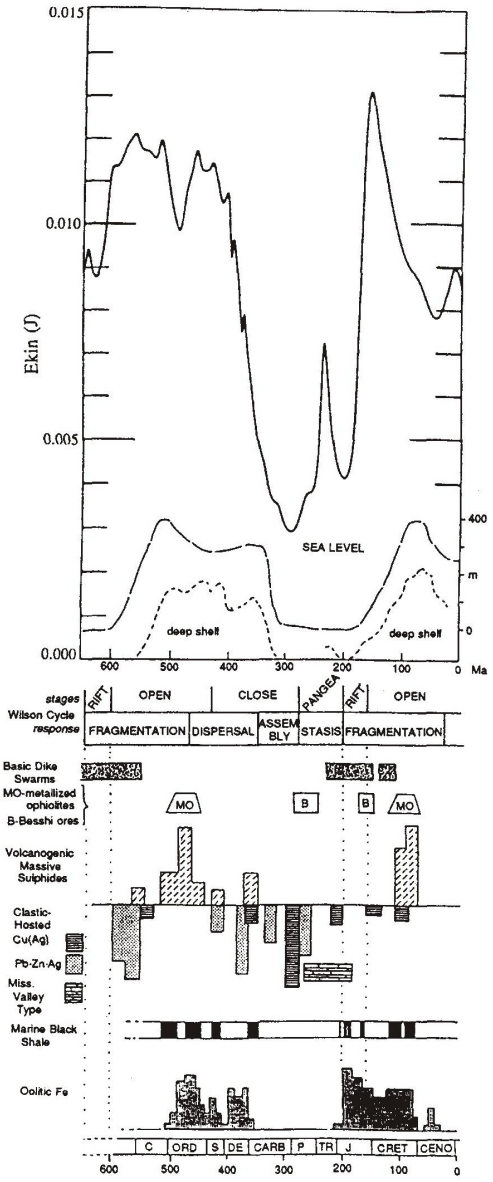

Fig. 11. Comparison of our curve of kinetic energy of mantle convection with Wilson cycle phenomena from Nance et al. (1986) and with the stratabound ore distribution after Titley (1993), plotted vs. time.

dependence of the kinetic energy of mantle convection. In particular, for oolitic iron ore, marine black shale and volcanogenic massive sulphides, there exists a close correlation with the principal maxima of the E_{kin} curve. The retardation of the clastic-hosted ores with respect to the volcanogenic massive sulphide ores is quite understandable in view of the way in which they have been produced.

4. Conclusions

Within the framework of the new formation of continents from mantle material, certain mantle volumes are left over, which are depleted with respect to incompatible elements and, thus, also with respect to uranium, thorium and potassium. As these three elements are the major heat-producing elements of the Earth's mantle, this will have an influence on thermal mantle convection. The continents themselves, too, influence the convection flows through their lateral displaceability, their thermal conductivity and their own heat production density. The majority of mineral age dates for the continents relate, however, to recycled continent material: through the lateral accretion of rhyolitic material from terranes and island arcs to the continents as well as through anatexis and regional metamorphosis, new orogenic ranges, mostly consisting of old continent material, are generated and are only partly complemented by andesitic volcanism and plutonism from the mantle (or its cold external skin, the oceanic lithosphere). These basic facts, the temperature dependence of mantle viscosity, and the considerable impenetrability of the endogenic phase transition at a depth of 670 km have been represented in a simple two-dimensional thermal convection model with chemical segregation. This means that both the heat source density and viscosity are variable with respect to space and time in the model. There are solutions involving physically acceptable parameters, which provide for a reasonable description of the heat flux and of the distribution of the convective flow velocities, temperature and viscosity. The convective vigour exhibits time episodic variations, the behaviour of which is roughly in agreement with the distribution of the Wilson cycles, the distribution of the mineral date abundances, the sea-level variations, and variations in the concentrations of certain elements and isotopes.

Acknowledgements

We wish to thank Harro Schmeling very much for placing his 2D thermal convection codes at our disposal and for extensive discussions. We used that code as a basis for the development of the code for a thermal convection with chemical segregation. We thank M. Ogawa and anonymous reviewers of an earlier version of this paper for helpful suggestions.

Appendix A

To make the calculations comprehensible, a few details will be given in the following. The specific internal energy u^* has been eliminated, using the first law of thermodynamics. In Eq. (7), we have assumed $k_2 = 29$ and $k_1 = 5 \times 10^7$. The heat flux vector, the specific heat production and the heat produced per unit time per unit space are designated by $\boldsymbol{q}$ ($\mathrm{W\,m^{-2}}$), H ($\mathrm{W\,kg^{-1}}$), and Q ($\mathrm{W\,m^{-3}}$), respectively. Now, non-dimensional variables are introduced. The subscript $_o$ designates a reference state of the system. Primes represent here non-dimensional variables. They are omitted, starting from Eq. (8).

$$\rho = \rho_o \rho'; \quad x = h \cdot x'; \quad z = h \cdot z'; \quad v_k = \frac{\kappa}{h} v'_k;$$

$$t = \frac{h^2}{\kappa} t'$$

$$p = \frac{\kappa \eta_o}{h^2} p' - \rho_o g h z'; \quad \tau_{ij} = \frac{\kappa \eta_o}{h^2} \tau'_{ij}; \quad \eta = \eta_o \eta'$$

$$T = \Delta T_o \cdot T' + T_o; \quad \psi = \psi' \kappa$$

$$H = \frac{c_p \cdot \Delta T_o \cdot \kappa}{h^2} H';$$

$$\text{amount of heat flux } q = \frac{c_p \cdot \Delta T_o \cdot \kappa \cdot \rho_o}{h} q'$$

$$T_m = \Delta T_o \cdot T'_m + T_o$$

The following parameters were used:

Depth of the layer	$h = 2.891 \times 10^6$ m
Thermal diffusivity of the mantle	$\kappa = 2.5 \times 10^{-6}$ m^2 s^{-1}
Thermal diffusivity of the crust	$\kappa_c = 0.6 \times 10^{-6}$ m^2 s^{-1}
Coefficient of thermal expansion	$\alpha = 1.4 \times 10^{-5}$ K^{-1}
Gravitational acceleration	$g = 9.81$ m s^{-2}
Reference densities:	
of the primitive mantle	$\rho_0 = 3.984 \times 10^3$ kg m^{-3}
of the continental crust	$\rho_0 = 2.900 \times 10^3$ kg m^{-3}
of the first residue (Res 1)	$\rho_0 = 4.003 \times 10^3$ kg m^{-3}
Specific heat at constant pressure	$c_p = 1.26 \times 10^3$ J K^{-1} kg^{-1}.

The remaining constants differ from model to model or from run to run. ρ_0 is the density at reference temperature T_0, η_0 is a reference shear viscosity, and ΔT_0 is a reference temperature contrast.

Now, some explanatory remarks follow on the idea and the algorithm of the simplified chemical segregation. The quantity $a_{\mu\nu}^{(1)}$ designates the initial abundance of the radionuclide ν (in ppm) according to Table 1. For instance, $\nu = 4$ stands for ^{238}U. The superscript (1) signifies the primordial mantle (see Table 2). All values of $a_{\mu\nu}$ have been multiplied by the intensification factor k_8 to obtain the correct average surface heat flow for today. Consequently, the quantity k_8 has not been varied to fit the curve $E_{kin}(t)$ to the Wilson cycle but to fit the computed average heat flow of the geological present to the measurements of the heat flow. For the adjusted heat flow, however, we obtain a good correspondence of the E_{kin} curve with the Wilson cycle. This is a strong argument for the model. In spite of the introduction of the intensification factor k_8, the model evolution has led to a depleted upper mantle for the present.

This is in concordance with the prevailing geochemical conceptions. After substituting the abundances $a_{\mu\nu}$ into Eq. (10), we obtain the specific heat production H, which is inserted into the differential equations of the solid-state convection of the mantle, Eq. (8) and Eq. (9). The specific heat production has an influence on the bulk mantle convective mass flow by thermal buoyancy. If, in addition, parts of the mantle are partly melted, a large percentage of the incompatible elements migrates into the melt, including the four major heat-producing radionuclides. The melt rises quickly in comparison with the velocity of the solid-state convection. The ascent of the melt is modelled as instantaneous rise. The melt becomes a contribution to the lithosphere, where it solidifies. We model this process by taking the tracers of the model as substitutes for the radionuclides. If the viscosity has fallen below a certain critical value in a sufficiently large partial volume of the mantle, we assume a segregation of the primordial mantle material into depleted mantle material and continental material at least with respect to the radiogenic heat sources in this volume. In this procedure, we use the abundances of Hofmann (1988).

The Type 1 tracers will be transformed into Type 4 tracers in the low-viscosity segregation volume (see Table 2). The original abundance of the radionuclides was $k_8 \cdot a_{\mu\nu}^{(1)}$ in the segregation volume. It dropped to $a_{\mu\nu}^{(4)}$ by segregation. On the other hand, rhyolitic terranes with abundances $a_{\mu\nu}^{(3)}$ developed at places near the surface above the segregation volume where originally primordial mantle material with abundances $k_8 \cdot a_{\mu\nu}^{(1)}$ was situated, too. The differences $(a_{\mu\nu}^{(3)} - k_8 \cdot a_{\mu\nu}^{(1)})$ are greater than the differences $(k_8 \cdot a_{\mu\nu}^{(1)} - a_{\mu\nu}^{(4)})$ in the segregation volume beneath. The rhyolitic terranes are considered to be the building blocks of the future continents. We need exactly $z_{\mu\nu}^*$ tracers in the segregation area to create one continental tracer above. Therefore we have

$$z_{\mu\nu}^* \left[k_8 \cdot a_{\mu\nu}^{(1)} - a_{\mu\nu}^{(4)} \right] = a_{\mu\nu}^{(3)} - k_8 \cdot a_{\mu\nu}^{(1)}$$

where $\nu = 1, 2, 3, 4$.

The formula applies to conserve the number of unstable parent atoms plus daughter atoms. In this way, we receive Eq. (11). We introduced $z_{\mu\nu} = \text{round}(z_{\mu\nu}^*)$ because the number of tracers must be an integer. Attention must be paid to the fact that $z_{\mu\nu}$ is a function of k_8. Using Table 2, we have $z_{\mu\nu} = 156$ for $k_8 = 1$ irrespective of ν. The precise procedure for the simplified chemical segregation is as follows. If a Type 3 tracer arose from a Type 1 marker near

the surface, then $z_{\mu\nu}^{(4)}$ Type 4 tracers should result from Type 1 tracers in the mantle beneath, where

$$z_{\mu\nu}^{(4)}(k_8) = \frac{a_{\mu\nu}^{(3)} - k_8 \cdot a_{\mu\nu}^{(1)}}{k_8 \cdot a_{\mu\nu}^{(1)} - a_{\mu\nu}^{(4)}}$$

A normalizing factor $[z_{\mu\nu}^{(4)}(1)]/[6 \cdot z_{\mu\nu}^{(4)}(k_8)]$ has been introduced to keep the number of the evolving Type 4 tracers constant irrespective of the different k_8 values. The numbers of the evolving Type 4 markers and Type 3 markers per time step are

$$rz_{\mu\nu}^{(4)} = \text{round}\left[z_{\mu\nu}^{(4)}(1)/6 \right] = 26$$

and

$$rz_{\mu\nu}^{(3)}(k_8) = \text{round}\left[\frac{z_{\mu\nu}^{(4)}(1)}{6 \cdot z_{\mu\nu}^{(4)}(k_8)} \right]$$

$$= \text{round}\left[\frac{a_{\mu\nu}^{(3)} - a_{\mu\nu}^{(1)}}{a_{\mu\nu}^{(1)} - a_{\mu\nu}^{(4)}} \cdot \frac{k_8 \cdot a_{\mu\nu}^{(1)} - a_{\mu\nu}^{(4)}}{a_{\mu\nu}^{(3)} - k_8 \cdot a_{\mu\nu}^{(1)}} / 6 \right]$$

respectively. We used the numbers for $\nu = 4$.

The markers are converted as follows. The procedure is described per time step. A Type 1 marker, in whose assigned mesh point $\eta(T) < f_6$ applies, is designated as Type 1 marker with $\eta < f_6$. Initially, each Type 1 marker m_i with $\eta < f_6$ of the upper mantle is checked to see whether it can form the centre of a segregation rectangle: a search rectangle around m_i has a height h_r and a breadth $h_r \cdot a_r$ using a fixed $a_r = 2$. The initial height was a dimensionless $\epsilon = 0.1$. The search rectangle is enlarged stepwise until the upper mantle is encircled entirely by the last rectangle. The area of each subsequent rectangle is enlarged by the area of the initial search rectangle. It is checked for each enlargement step to see whether at least $rz_{\mu\nu}^{(4)}$ Type 1 markers with $\eta < f_6$ are situated inside the search rectangle. In this case, the search is finished for the actual tracer m_i. If it is not possible to find enough Type 1 markers with $\eta < f_6$ or if their percentage (referred to the number of all markers in the search rectangle) is smaller than 50% then we proceed to the next marker. Otherwise, it will be checked whether the height of the found rectangle is smaller than $h_{r,min}$. At the beginning of the time step, $h_{r,min}$ has been to set 10^{40} formally. $h_{r,min}$ will be altered to the height h_r of the found rectangle only if it is smaller than the previous $h_{r,min}$. Simultaneously, the first found $rz_{\mu\nu}^{(4)}$ Type 1 markers with $\eta < f_6$ will be stored as a possible cluster of future converted markers. Now we proceed unconditionally to the next marker. If all upper-mantle markers have been checked in this way and no possible cluster of future converted markers has been found, then we proceed to the next time step. Otherwise, the centre of gravity of the smallest cluster will be projected perpendicularly onto the surface. This point is designated as P'. The $rz_{\mu\nu}^{(4)}$ Type 1 markers located next to P', which are also located in a subsurface layer with a thickness of $D_c = 100$ km, are then transformed into Type 3 markers. Finally, the Type 1 markers of the cluster in the mantle below are converted into Type 4 markers if enough Type 1 markers for the conversion to Type 3 markers have been found in the D_c-layer.

Appendix B

The computed convection–segregation mechanism has several constituent parts, connected in a complex manner: the chemical segregation of the primordial mantle which leaves behind depleted mantle reservoirs, the radiogenic heating from within, a strong temperature dependence of the shear viscosity, and the primordial heat. The last has been expressed by an assumed initial distribution of temperature which follows from extensive considerations on the accretion of the Earth, details of which will be published in a separate paper (Walzer and Hendel, 1997).

1. The chemical fractionation is important to the determination of the kinetic-energy fluctuations of the mantle convection. The kinetic energy is a measure of the vigour of convection.
2. One could presume that the episodicity is an artefact. This supposition is wrong.

Both propositions, (1) and (2), can be proved by repeating the computer runs with the same parameters but with a disconnected segregation subroutine. In this sense, Fig. 12 is the exact companion result to

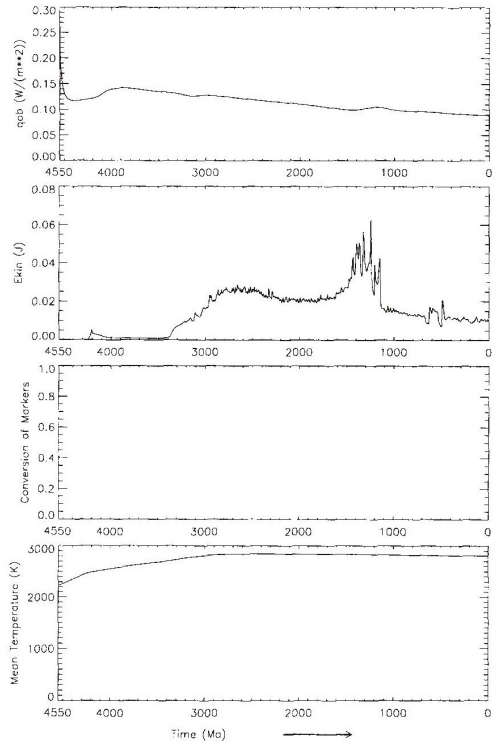

Fig. 12. The results of the model system without chemical segregation. Description of panels as for Fig. 1. (For explanation, see Appendix B.)

Fig. 1 but without fractionation. The course of the mean temperature (fourth panel) is scarcely altered. The averaged surface heat flow (first panel) is slightly lowered and has a similar course as a function of time. According to the assumption, the curve of the conversion of markers vanishes (third panel). Comparing the second panels of Fig. 1 and Fig. 12, we arrive at the following conclusions. Although the small steps at 4240 and 3370 Ma are connected with the total system without chemical fractionation and are, of course, partly determined by the initial conditions, the large peaks at 2350 Ma and younger ages appear only in the system with chemical segregation. Even the small maximum at 4200 Ma is higher in Fig. 1. The synchronous large peak in the curve of the conversion of markers verifies the assumption that even the small E_{kin} peak at 4200 Ma in Fig. 1 is influenced by fractionation.

References

Abbot, D., Burgess, L., Longhi, J. and Smith, W.H.F., 1994. An empirical thermal history of the Earth's upper mantle. J. Geophys. Res., 99(B7): 13835–13850.

Akaogi, M. and Ito, E., 1993. Refinement of enthalpy measurement of $MgSiO_3$ perovskite and negative pressure–temperature slopes for perovskite-forming reactions, Geophys. Res. Lett., 20: 1839–1842.

Billington, S., 1978. The morphology and tectonics of subducted lithosphere in the Tonga–Fiji–Kermadec region from seismicity and focal mechanism solutions. Ph.D. Thesis, Cornell University, Ithaca, NY.

Christensen, U.R., 1984. Convection with pressure- and temperature-dependent non-Newtonian rheology. Geophys. J. R. Astron. Soc., 77: 343–384.

Christensen, U.R. and Yuen, D.A., 1989. Time-dependent convection with non-Newtonian viscosity. J. Geophys. Res., 94: 814–820.

Condie, K.C., 1989. Plate Tectonics and Crustal Evolution, 3rd edn. Pergamon, Oxford, 476 pp.

Dasch, E.J., Ryder, G. and Nyquist, L.E., 1988. Chronology and complexity of early lunar crust. Tectonophysics, 161: 157–164.

Gastil, G., 1960. The distribution of mineral dates in time and space. Am. J. Sci., 258: 1–35.

Gurnis, M., 1988. Large-scale mantle convection and the aggregation and dispersal of supercontinents. Nature, 332(6166): 695–699.

Hallam, A., 1984. Pre-Quaternary sea-level changes. Annu. Rev. Earth Planet. Sci., 12: 205–243.

Hansen, U. and Ebel, A., 1988. Time-dependent thermal convection—a possible explanation for a multiscale flow in the Earth's mantle. Geophys. J., 94: 181–191.

Harland, W.B., 1983. The Proterozoic glacial record. Mem. Geol. Soc. Am., 161: 279–288.

Heinz, D.L. and Jeanloz, R., 1987. Measurement of the melting curve of $Mg_{0.9}Fe_{0.1}SiO_3$ at lower mantle conditions and its geophysical implications. J. Geophys. Res., 92: 11437–11444.

Hofmann, A.W., 1988. Chemical differentiation of the Earth: the relationship between mantle, continental crust, and oceanic crust. Earth Planet. Sci. Lett., 90: 297–314.

Hoffman, P.F., 1990. Supercontinents. In: W.A. Nierenberg (Editor), Encyclopedia of Earth System Science. Academic Press, San Diego, CA, pp. 323–328.

Ito, E. and Takahashi, E., 1987. Melting of peridotite at uppermost mantle conditions. Nature, 328: 514–517.

James, H.L., 1983. Distribution of banded iron-formations in space and time. In: A.F. Trendall and R.C. Morris (Editors), Iron-Formations: Facts and Problems. Elsevier, Amsterdam, pp. 471–490.

Knittle, E. and Jeanloz, R., 1989. Melting curve of (Mg,Fe)SiO_3

perovskite to 96 GPa: evidence for a structural transition in lower mantle melts. Geophys. Res. Lett., 16: 421–424.

Lovelock, J.E. and Whitfield, M., 1982. Life span of the biosphere. Nature, 296: 561–563.

Machetel, P. and Weber, P., 1991. Intermittent layered convection in a model mantle with an endothermic phase change at 670 km. Nature, 350: 55–57.

Marzocchi, W., Mulargia, F. and Paruolo, P., 1992. The correlation of geomagnetic reversals and mean sea level in the last 150 m.y. Earth Planet. Sci. Lett., 111: 383–393.

Merrill, R.T. and McFadden, P.L., 1990. Paleomagnetism and the nature of the geodynamo. Science, 248: 345–350.

Nance, R.D., Worsley, T.R. and Moody, J.B., 1986. Post-Archean biogeochemical cycles and long-term episodicity in tectonic processes. Geology, 14: 514–518.

Nance, R.D., Worsley, T.R. and Moody, J.B., 1988. The supercontinent cycle. Sci. Am., 259(1): 44–51.

Ogawa, M., 1988. Numerical experiments on coupled magmatism–mantle convection system: implications for mantle evolution and Archean continental crusts. J. Geophys. Res., 93(B12): 15119–15134.

Ogawa, M., 1993. A numerical model of a coupled magmatism–mantle convection system in Venus and the Earth's mantle beneath Archean continental crusts. Icarus, 102: 40–61.

Ogawa, M., 1994. Effects of chemical fractionation of heat-producing elements on mantle evolution inferred from a numerical model of coupled magmatism–mantle convection system. Phys. Earth Planet. Inter., 83: 101–127.

Patchett, P.J. and Arndt, N.T., 1986. Nd isotopes and tectonics of 1.9–1.7 Ga crustal genesis. Earth Planet. Sci. Lett., 78: 329–338.

Pollack, H.N., Hurter, S.J. and Johnson, J.R., 1993. Heat flow from the Earth's interior: analysis of the global data set. Rev. Geophys., 31: 267–280.

Rampino, M.R. and Caldeira, K., 1993. Major episodes of geologic change: correlations, time structure and possible causes. Earth Planet. Sci. Lett., 114: 215–227.

Ranalli, G., 1991. The microphysical approach to mantle rheology. In: R. Sabadini, K. Lambeck and E. Boschi (Editors), Glacial Isostasy, Sea-Level and Mantle Rheology. Kluwer Academic, Dordrecht, pp. 343–378.

Ritzert, M. and Jacoby, W.R., 1992. The geoid signal of 2-D convection with temperature and pressure-dependent rheology. J. Geodyn., 16: 81–102.

Rogers, J.J.W., Unrug, R. and Sultan, M., 1995. Tectonic assembly of Gondwana. J. Geodyn., 19: 1–34.

Ronov, A.B., Migdisov, A.A. and Barskaya, N.V., 1969. Some regularities in the development of sedimentary rocks and of the palaeogeographic conditions of sedimentation on the Russian platform. Litol. Polezn. Iskop., 6: 3.

Schmeling, H. and Bussod, G.Y., 1996. Variable viscosity convection and partial melting in the continental asthenosphere. J. Geophys. Res., 101: 5411–5423.

Schmeling, H. and Marquart, G., 1993. Mantle flow and the evolution of the lithosphere. Phys. Earth Planet. Inter., 79: 241–267.

Şengör, A.M.C., 1990. Plate tectonics and orogenic research after 25 years: a Tethyan perspective. Earth-Sci. Rev., 27: 1–201.

Sloss, L.L., 1964. Tectonic cycles of the North American craton. State Geol. Surv. Kans. Bull., 169(2): 449–460.

Spohn, T. and Breuer, D., 1993. Mantle differentiation through continental crust growth and recycling and the thermal evolution of the Earth. IUGG Vol. 14, Geophys. Monogr. Am. Geophys. Union, 74: 55–71.

Stille, H., 1944. Geotektonische Gliederung der Erdgeschichte. Abh. Preuss. Akad. Wiss., Math. Naturwiss. Kl., 3: 1–80.

Sutton, J., 1967. The extension of the geological record into the Pre-Cambrian. Proc. Geol. Assoc., 78: 493–534.

Tackley, P.J., Stevenson, D.J., Glatzmaier, G.A. and Schubert, G., 1993. Effects of an endothermic phase transition at 670 km depth on spherical mantle convection. Nature, 361: 699–704.

Titley, S.R., 1993. Relationship of stratabound ores with tectonic cycles of the Phanerozoic and Proterozoic. Precambrian Res., 61: 295–322.

Vail, P.R. and Todd, R.G., 1980. Northern North Sea Jurassic unconformities, chronostratigraphy and sea-level changes from seismic stratigraphy. In: Proc. Petroleum Geology of the Continental Shelf of North-West Europe Conf., 4–7 March 1980, London, pp. 216–235.

Vail, P.R., Mitchum, R.M., Todd, R.G., Widmier, J.M. et al., 1977. Seismic stratigraphy and global changes of sea level. Mem. Am. Assoc. Pet. Geol., 26: 49–212.

Van Schmus, W.R., 1989. Radioactivity properties of minerals and rocks. In: R.S. Carmichael (Editor), Practical Handbook of Physical Properties of Rocks and Minerals. CRC Press, Boca Raton, FL, pp. 583–596.

Walzer, U., 1981. Untersuchung der Konvektion im Erdinneren und dafür wichtiger Materialparameter unter hohem Druck. Veröff. Zentralinst. Phys. Erde, 75: 1–256.

Walzer, U. and Hendel, R., 1997. Time-dependent thermal convection, mantle differentiation and continental crust growth, in preparation.

Warren, P.H., 1989. Growth of the continental crust: a planetary mantle perspective. Tectonophysics, 161: 165–199.

Windley, B.F., 1984. The Evolving Continents, 2nd edn. Wiley, New York, 399 pp.

Worsley, T.R., Nance, R.D. and Moody, J.B., 1986. Tectonic cycles and the history of the Earth's biogeochemical and paleoceanographic record. Paleoceanography, 1: 233–263.

Zhong, S. and Gurnis, M., 1994. Controls on trench topography from dynamic models of subducted slabs. J. Geophys. Res., 99(B8): 15683–15695.